Novel Alternating Fluorene-Based Conjugated Polymers Containing Oxadiazole Pendants with Various Terminal Groups

Hsiao-Hsien Sung and Hong-Cheu Lin*

Department of Materials Science and Engineering, National Chiao Tung University, Hsinchu, Taiwan, ROC

Received May 21, 2004; Revised Manuscript Received August 9, 2004

ABSTRACT: A series of soluble alternating fluorene-based copolymers containing symmetrical and asymmetrical 1,3,4-oxadiazole (OXD) pendants with various terminal groups are synthesized by the palladium-catalyzed Suzuki coupling reaction. These polymers possess higher glass transition temperatures than that of the analogous dialkoxy-substituted polymer ($PFPOC_6$) consisting of the same backbone without OXD pendants. The photophysical and electrochemical properties of these polymers are affected by the polar effect (electron-withdrawing group, −CN, and electron-donating group, −R or −OR) and the size effect (the size of the grafted side chain) of the OXD pendants. Owing to the large steric hindrance of OXD pendants, the aggregation of these polymers in solids is reduced, which results in almost identical PL emissions in both solution and solid states. The bulky OXD pendants on the polymer side chains can provide the polymer films with lower HOMO and LUMO energy levels and better electron injection property. Since only one emission peak is observed in both PL and EL spectra of these polymers, it is evidenced that effective energy transfer from the OXD pendants to the conjugated polymer backbones has occurred, thus eliminating the light emission from the OXD pendants. These asymmetrical OXD-substituted polymers have higher quantum yields and less aggregation in the solid state than the symmetrical OXD-substituted polymers. The symmetrical OXD-substituted polymer (**P1**) has a longer PL emission wavelength than the asymmetrical OXD-substituted polymers (**P2**−**P8**), which may be due to the improvement of the coplanarity between the polymer backbone and the symmetrical OXD pendants and/or the introduction of two electron-withdrawing OXD pendants.

Introduction

Polymer light-emitting diodes (PLEDs) have been studied intensively during the past decade because of their potential applications in a new generation of flat display and lighting technologies.[1,2] Compared with inorganic electroluminescent (EL) materials, π-conjugated polymers have many virtues such as ease of forming large area, mechanical flexibility, low fabrication cost, and easy color tuning through molecular engineering.[3] Therefore, it is generally expected that PLEDs will be a possible candidate of the next generation display technology.

To obtain highly efficient PLED devices, a balance in the injection and transportation of both holes and electrons into the polymer emissive layer is necessary.[4−8] However, most EL polymers inject and transport holes more efficiently than electrons due to the inherent richness of π-electrons in the EL polymers, which results in an unbalance of opposite carrier currents and a shift of the recombination zone toward the region near the interface of the polymer and the cathode. Thus, the synthesis of efficient electron-transporting polymers is needed to improve EL device performance. Polymers containing electron-withdrawing units in the main chains or side chains usually have large electron affinities. In recent years, polyquinolines, polyquinoxalines, polybenzobisazoles, and polypyridines have been demonstrated as electron-transporting (ET) polymers due to the good film quality and the excellent thermal and oxidative stability.[9−11] Molecular and polymeric 2,5-diphenyl-1,3,4-oxadiazolediyl derivatives are the most widely studied classes of electron-injection and/or hole-blocking materials[12] by virtue of many merits owned by 1,3,4-oxadiazole (OXD) moieties, such as prominent electron affinity, high photoluminescence (PL) quantum yield, and good thermal stability.[13] On the other hand, to achieve highly efficient and luminescent PLED devices, it is important to suppress the self-quenching process, which originates from the formation of excimers due to the intermolecular interactions in the solid state. Since large steric hindrance of lateral substitution will cause the decrease of crystallinity in the resulting polymers, the bulky substitution with symmetrical and asymmetrical structure on the side chains of the polymer can provide the polymer film with an amorphous property.[14] In addition, the pseudo-orthogonal arrangement of the rigid pendant groups can reduce the π-stacking and thus increase the radiative decay quantum efficiency and photostability of the polymers.[12c,15] In this paper, we report a series of alternating fluorene-based copolymers containing symmetrical and asymmetrical substituted OXD pendants with different terminal groups (on the side chains of the polymers). The electrochemical, spectroscopic, and thermal properties of these polymers with respect to various terminal OXD groups are also investigated in this study.

Experimental Section

Measurements. ^{1}H NMR spectra were recorded on a Varian Unity 300 MHz spectrometer using $CDCl_3$ solvent. Elemental analyses were performed on a HERAEUS CHN-OS RAPID elemental analyzer. Transition temperatures were determined by differential scanning calorimetry (Perkin-Elmer Pyris 7) with a heating and cooling rate of 10 °C/min. Thermogravimetric analysis (TGA) was conducted on a Du Pont Thermal Analyst 2100 system with a TGA 2950 thermogravimetric analyzer under a heating rate of 20 °C/min. Gel

* Author for correspondence: Tel 8863−5712121 ext 55305; Fax 8863-5724727; e-mail linhc@cc.nctu.edu.tw.

10.1021/ma0489927 CCC: $27.50
Published on Web 09/23/2004

Scheme 1. Synthetic Routes of Monomers

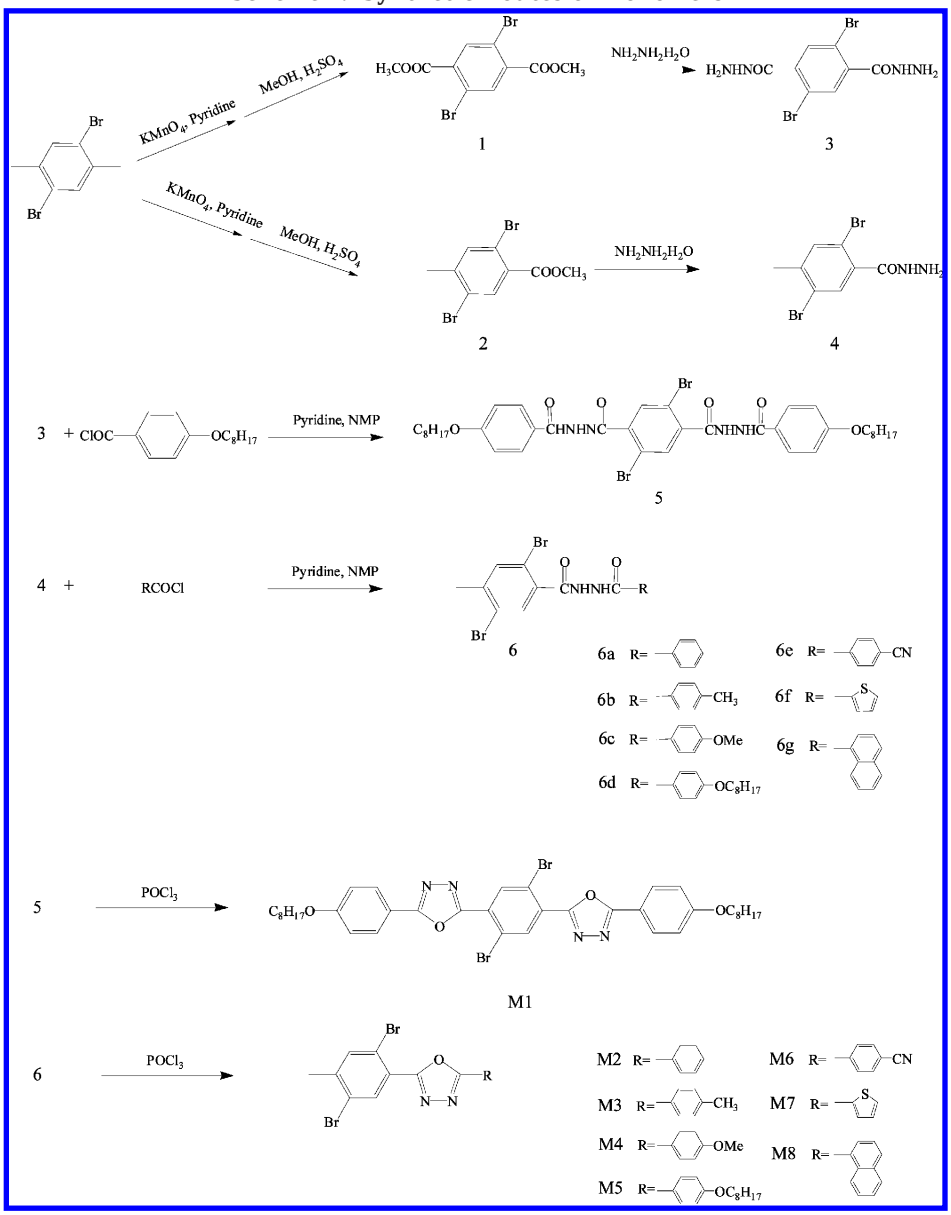

permeation chromatography (GPC) analysis was conducted on a Waters 1515 separation module using polystyrene as a standard and THF as an eluant. UV−vis absorption spectra were recorded in dilute chloroform solutions (10^{-5} M) on a HP G1103A spectrophotometer, and fluorescence spectra were obtained on a Hitachi F-4500 spectrophotometer. Fluorescence quantum yields were determined by comparing the integrated PL density of a reference 9,10-diphenylanthracene in toluene with a known quantum yield (ca. 5×10^{-6} M, quantum yield = 1.0). Cyclic voltammetry (CV) was performed at a scanning rate of 100 mV/s on a BAS 100 B/W electrochemical analyzer, which was equipped with a three-electrode cell. Pt wire was used as a counter electrode, and an Ag/AgCl was used as a reference electrode in the CV measurement. The polymer thin film was cast onto a Pt disk as a working electrode with ferrocene as a standard in actonitrile, and 0.1 M tetrabutylammonium hexafluorophosphate ($TBAPF_6$) was used as a supporting electrolyte. Polymer thin films were spin-coated on a quartz substrate from chloroform solution with a concentration of 10 mg/mL (this condition consists with the electroluminescent device).

Materials. Chemicals and solvents were reagent grades and purchased from Aldrich, ARCROS, TCI, and Lancaster Chemical Co. Dichloromathane and THF were distilled to keep anhydrous before use. The other chemicals were used without further purification.

The synthetic routes of monomers **M1**−**M8** are shown in Scheme 1. First, 2,5-dibromo-*p*-xylene was oxidized with potassium permanganate in pyridine to afford 2,5-dibromoterephthalic acid and 2,5-dibromo-4-methylbenzoic acid. After then, the acid group was further esterified to give 2,5-dibromoterephthalic acid dimethyl ester (**1**) and 2,5-dibromo-4-methylbenzoic acid methyl ester (**2**), which were synthesized by the modified procedure of ref 16. After the ester groups had been converted to benzoyl hydrazides (**3** and **4**), they were reacted with various aryl chloride to form compounds **5** and **6**. Finally, monomers **M1**−**M8** were produced by the dehydrative cyclization of hydrazides in $POCl_3$.

2,5-Dibromoterephthaloyldihydrazides (3). A mixture of 3.19 g (9.07 mmol) of methyl-2,5-dibromoterephthalate and 4.53 g (90.70 mmol) of hydrazine monohydrate was dissolved in 35 mL of methanol and then refluxed for 24 h. After cooling, the product was poured into water and recrystallized from methanol. Yield: 83%. ^{1}H NMR (ppm, DMSO-d_6): 4.51 (s, 4H), 7.58 (s, 2H), 9.69 (s, 2H).

2,5-Dibromo-4-methylbenzoic Acid Hydrazide (4). Yield: 78%. ^{1}H NMR (ppm, DMSO-d_6): 2.33 (s, 3H), 7.52 (s, 1H), 7.68 (s, 1H), 9.57 (s, 1H).

Compound 5. 0.81 g (3.02 mmol) of 4-octyloxybenzoyl chloride was added into a solution containing 0.53 g (1.51 mmol) of **1** and 0.25 mL (3.02 mmol) of pyridine in 10 mL of NMP. The reaction mixture was stirred for 12 h and then

Scheme 2. Synthetic Route of Polymers

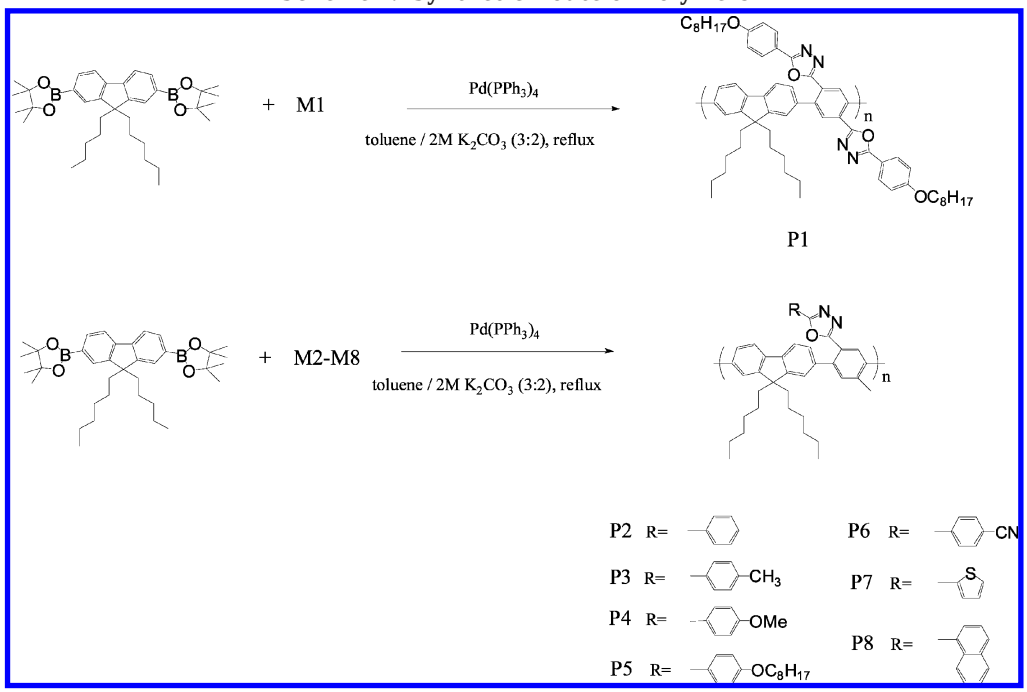

poured into water. The product was filtered and crystallized from methanol. Yield: 73%. ^{1}H NMR (ppm, DMSO-d_6): 0.83 (t, 6H), 1.21−1.80 (m, 24H), 4.04 (t, 4H), 7.02 (d, J = 9 Hz, 4H), 7.78 (s, 2H), 7.89 (d, J = 8.7 Hz, 4H), 10.55 (s, 2H), 10.58 (s, 2H).

Benzoic Acid *N*-(2,5-Dibromo-4-methyl-benzoyl)hydrazide (6−2). Yield: 81%. ^{1}H NMR (ppm, DMSO-d_6): 2.38 (s, 3H), 7.49−7.62 (m, 3H), 7.68 (s, 1H), 7.77 (s, 1H), 7.91 (d, J = 8.4 Hz, 2H), 10.38 (s, 1H), 10.44 (s, 1H).

4-Methylbenzoic Acid *N*′-(2,5-dibromo-4-methylbenzoyl)hydrazide (6−3). Yield: 66%. ^{1}H NMR (ppm, DMSO-d_6): 2.37 (s, 3H), 2.38 (s, 3H), 7.30 (d, J = 8.1 Hz, 2H), 7.68 (s, 1H), 7.76 (s, 1H), 7.84 (d, J = 7.5 Hz, 2H), 10.40 (s, 1H), 10.58 (s, 1H).

4-Methoxybenzoic Acid *N*′-(2,5-dibromo-4-methylbenzoyl)hydrazide (6−4). Yield: 88%. ^{1}H NMR (ppm, DMSO-d_6): 2.38 (s, 3H), 3.82 (s, 3H), 7.03 (d, J = 8.7 Hz, 2H), 7.68 (s, 1H), 7.76 (s, 1H), 7.90 (d, J = 8.7 Hz, 2H), 10.36 (s, 1H), 10.51 (s, 1H).

4-Octyloxybenzoic Acid *N*′-(2,5-dibromo-4-methylbenzoyl)hydrazide (6−5). Yield: 79%. ^{1}H NMR (ppm, DMSO-d_6): 0.83 (t, 3H), 1.25−1.79 (m, 12H), 2.38 (s, 3H), 4.03 (t, 2H), 7.00 (d, J = 8.7 Hz, 2H), 7.68 (s, 1H), 7.76 (s, 1H), 7.87 (d, J = 9 Hz, 2H), 10.37 (s, 1H), 10.50 (s, 1H).

4-Cyanobenzoic Acid *N*′-(2,5-Dibromo-4-methylbenzoyl)hydrazide (6−6). Yield: 82%. ^{1}H NMR (ppm, DMSO-d_6): 2.38 (s, 3H), 7.67 (s, 1H), 7.77 (s, 1H), 8.00 (d, J = 8.4 Hz, 2H), 8.05 (d, J = 8.1 Hz, 2H), 10.59 (s, 1H), 10.97 (s, 1H).

Thiophene-2-carboxylic Acid *N*′-(2,5-dibromo-4-methylbenzoyl)hydrazide (6−7). Yield: 63%. ^{1}H NMR (ppm, DMSO-d_6): 2.38 (s, 3H), 7.20 (t, J = 5.1 Hz, 1H), 7.65 (s, 1H), 7.77 (s, 1H), 7.86 (d, J = 9.3 Hz, 1H), 7.88 (d, J = 8.4 Hz, 1H), 10.47 (s, 1H), 10.71 (s, 1H).

Naphthalene-1-carboxylic Acid *N*′-(2,5-dibromo-4-methylbenzoyl)hydrazide (6−8). Yield: 71%. ^{1}H NMR (ppm, DMSO-d_6): 2.39 (s, 3H), 7.56−7.78 (m, 6H), 8.00 (d, J = 7.2 Hz, 1H), 8.06 (d, J = 7.2 Hz, 1H), 8.36 (d, J = 8.7 Hz, 1H), 10.58 (s, 1H), 10.64 (s, 1H).

Monomer 1 (M1). 0.8 g (1.02 mmol) of **4a** was dissolved in 100 mL of $POCl_3$. The reaction mixture was heated to 130°C overnight and then cooled to room temperature. Most $POCl_3$ in reaction mixture was removed at reduced pressure and poured into water. The product was filtered and crystallized from methanol and chloroform several times to get a yellow solid. Yield: 74%. ^{1}H NMR (ppm, $CDCl_3$): 0.88 (t, 6H), 1.30−1.86 (m, 24H), 4.05 (t, 4H), 7.03 (d, J = 9 Hz, 4H), 8.08 (d, J = 8.7 Hz, 4H), 8.51 (s, 2H). Anal. Calcd for $C_{38}H_{44}Br_2N_{24}O_4$: C, 58.47; H, 5.68; N, 7.18. Found: C, 58.20; H, 5.79; N, 7.07.

2-(2,5-Dibromo-4-methylphenyl)-5-phenyl-[1,3,4]oxadiazole (M2). Yield: 56%. ^{1}H NMR (ppm, $CDCl_3$): 2.46 (s, 3H), 7.52−7.65 (m, 3H), 8.14−8.17 (m, 2H), 8.24 (s, 1H). Anal. Calcd for $C_{15}H_{10}Br_2N_2O$: C, 45.72; H, 2.56; N, 7.11. Found: C, 46.06; H, 2.87; N, 6.87.

2-(2,5-Dibromo-4-methylphenyl)-5-*p*-tolyl-[1,3,4]oxadiazole (M3). Yield: 68%. ^{1}H NMR (ppm, $CDCl_3$): 2.45 (s, 3H), 2.46 (s, 3H), 7.33 (d, J = 7.8 Hz, 2H), 7.64 (s, 1H), 8.02 (d, J = 8.4 Hz, 2H), 8.22 (s, 1H). Anal. Calcd for $C_{16}H_{12}Br_2N_2O$: C, 47.09; H, 2.96; N, 6.86. Found: C, 47.07; H, 3.23; N, 6.80.

2-(2,5-Dibromo-4-methylphenyl)-5-(4-methoxyphenyl)-[1,3,4]oxadiazole (M4). Yield: 44%. ^{1}H NMR (ppm, $CDCl_3$): 2.46 (s, 3H), 3.90 (s, 3H), 7.02 (d, J = 9 Hz, 2H), 7.64 (s, 1H), 8.07 (d, J = 8.7 Hz, 2H), 8.22 (s, 1H). Anal. Calcd for $C_{16}H_{12}Br_2N_2O_2$: C, 45.31; H, 2.85; N, 6.61. Found: C, 45.09; H, 3.09; N, 6.51.

2-(2,5-Dibromo-4-methylphenyl)-5-(4-octyloxyphenyl)-[1,3,4]oxadiazole (M5). Yield: 81%. ^{1}H NMR (ppm, $CDCl_3$): 0.90 (t, 3H), 1.20−1.51 (m, 10H), 1.77 (m, 2H), 2.46 (s, 3H), 4.04 (t, 2H), 7.00 (d, J = 8.7 Hz, 2H), 7.64 (s, 1H), 8.05 (d, J = 8.7 Hz, 2H), 8.22 (s, 1H). Anal. Calcd for $C_{23}H_{26}Br_2N_2O_2$: C, 52.89; H, 5.02; N, 5.36. Found: C, 53.13; H, 5.34; N, 5.30.

4-[5-(2,5-Dibromo-4-methylphenyl)-[1,3,4]oxadiazol-2-yl]benzonitrile (M6). Yield: 88%. ^{1}H NMR (ppm, $CDCl_3$): 2.48 (s, 3H), 7.67 (s, 1H), 7.84 (d, J = 8.4 Hz, 2H), 8.25 (s, 1H), 8.26 (d, J = 8.1 Hz, 2H). Anal. Calcd for $C_{16}H_9Br_2N_3O$: C, 45.86; H, 2.16; N, 10.03. Found: C, 45.82; H, 2.49; N, 10.07.

2-(2,5-Dibromo-4-methylphenyl)-5-thiophen-2-yl-[1,3,4]oxadiazole (M7). Yield: 88%. ^{1}H NMR (ppm, $CDCl_3$): 2.45 (s, 3H), 7.20 (t, J = 5.1 Hz, 1H), 7.59 (d, J = 5.1 Hz, 1H), 7.63 (s, 1H), 7.85 (d, J = 5.1 Hz, 1H), 8.19 (s, 1H). Anal. Calcd for $C_{13}H_8Br_2N_2OS$: C, 39.03; H, 2.02; N, 7.00. Found: C, 39.37; H, 2.34; N, 6.92.

2-(2,5-Dibromo-4-methylphenyl)-5-naphthalen-1-yl-[1,3,4]oxadiazole (M8). Yield: 68%. ^{1}H NMR (ppm, $CDCl_3$): 2.41 (s, 3H), 7.56−7.68 (m, 4H), 7.88−8.23 (m, 4H), 9.30 (d, J = 8.1 Hz, 1H). Anal. Calcd for $C_{19}H_{12}Br_2N_2O$: C, 51.38; H, 2.72; N, 6.31. Found: C, 51.32; H, 3.01; N, 6.28.

Polymerization. The synthetic routes of polymers **P1**−**P8** are shown in Scheme 2. The general procedure of polymerization is proceeded through the Suzuki coupling reaction. A mixture of 2,7-bis(4,4,5,5-tetramethyl-1,3,2-dioxaborolan-2-yl)-9,9-dioctylfluorene (1 equiv), dibromo compounds **M1**−**M8** (1 equiv), and tetrakis(triphenylphosphine)palladium (1.0 mol %)

Table 1. Molecular Weights and Thermal Properties of Polymers

polymer	yield (%)	M_n	PDI	T_d[a] (°C)	T_g[b] (°C)
P1	51	4 900	1.2	398	119
P2	23	6 700	1.7	418	109
P3	40	14 800	1.5	421	125
P4	35	26 600	2.8	414	128
P5	78	24 500	2.7	410	85
P6	54	25 200	2.6	422	148
P7	88	12 200	1.9	407	120
P8	63	6 500	1.7	446	132

[a] Temperature of 5% weight loss was measured by TGA in nitrogen. [b] The glass transition temperature (T_g) was measured on the first cooling cycle after the sample had been heated to 280 °C.

was added in a degassed mixture of toluene ([monomer] = 0.2 M) and aqueous 2 M potassium carbonate (3:2 in volume). The mixture was vigorously stirred and reacted at 87 °C for 72 h. After the mixture was cooled to room temperature, it was poured into 200 mL of methanol. A fibrous solid was obtained by filtration, and the solid was sequentially washed with methanol, water, and methanol.

P1. Yield: 51%. ^{1}H NMR (ppm, $CDCl_3$): 0.61−1.41 (m, 46H), 1.69−2.00 (m, 10H), 3.88 (br, 4H), 6.73 (d, J = 8.4 Hz, 4H), 7.37−7.55 (m, 8H), 7.81 (d, J = 7.2 Hz, 2H), 8.37 (s, 2H). Anal. Calcd for $C_{63}H_{76}N_4O_4$: C, 79.37; H, 8.04; N, 5.88. Found: C, 78.10; H, 7.97; N, 5.60.

P2. Yield: 23%. ^{1}H NMR (ppm, $CDCl_3$): 0.66−1.20 (m, 22H), 1.91 (br, 4H), 2.46 (s, 3H), 7.22−7.59 (m, 10H), 7.76−7.81 (m, 2H), 8.14 (s, 1H). Anal. Calcd for $C_{40}H_{42}N_2O$: C, 84.77; H, 7.47; N, 4.94. Found: C, 83.26; H, 7.45; N, 4.83.

P3. Yield: 40%. ^{1}H NMR (ppm, $CDCl_3$): 0.66−1.23 (m, 22H), 1.92 (br, 4H), 2.28 (s, 3H), 2.46 (s, 3H), 7.03 (d, J = 7.8 Hz, 2H), 7.36−7.50 (m, 7H), 7.74−7.82 (m, 2H), 8.12 (s, 1H). Anal. Calcd for $C_{41}H_{44}N_2O$: C, 84.79; H, 7.64; N, 4.82. Found: C, 83.44; H, 7.55; N, 4.62.

P4. Yield: 35%. ^{1}H NMR (ppm, $CDCl_3$): 0.74−1.26 (m, 22H), 2.1 (br, 4H), 2.48 (s, 3H), 3.77 (s, 3H), 6.75 (br, 2H), 7.41−7.84 (m, 9H), 8.14 (s, 1H). Anal. Calcd for $C_{41}H_{44}N_2O_2$: C, 82.51; H, 7.43; N, 4.69. Found: C, 81.42; H, 7.50; N, 4.48.

P5. Yield: 78%. ^{1}H NMR (ppm, $CDCl_3$): 0.68−1.41 (m, 35H), 1.74−2.07 (m, 6H), 2.47 (s, 3H), 3.90 (br, 2H), 6.77 (d, J = 8.4 Hz, 2H), 7.41−7.83 (m, 9H), 8.15 (s, 1H). Anal. Calcd for $C_{48}H_{58}N_2O_2$: C, 82.95; H, 8.41; N, 4.03. Found: C, 82.03; H, 8.27; N, 3.71.

P6. Yield: 54%. ^{1}H NMR (ppm, $CDCl_3$): 0.68−1.26 (m, 22H), 1.95 (br, 4H), 2.50 (s, 3H), 7.35−7.86 (m, 11H), 8.21 (s, 1H). Anal. Calcd for $C_{41}H_{41}N_3O$: C, 83.21; H, 6.98; N, 7.10. Found: C, 82.26; H, 6.91; N, 6.73.

P7. Yield: 88%. ^{1}H NMR (ppm, $CDCl_3$): 0.75−1.20 (m, 22H), 2.04 (br, 4H), 2.48 (s, 3H), 6.95 (br, 1H), 7.37−7.49 (m, 7H), 7.76−7.85 (m, 2H), 8.11 (s, 1H). Anal. Calcd for $C_{38}H_{40}N_2OS$: C, 79.68; H, 7.04; N, 4.89. Found: C, 78.47; H, 7.14; N, 4.69.

P8. Yield: 63%. ^{1}H NMR (ppm, $CDCl_3$): 0.48−1.20 (m, 22H), 1.92 (br, 4H), 2.48 (s, 3H), 7.12 (br, 1H), 7.39−7.55 (m, 8H), 7.80−7.87 (m, 4H), 8.20 (s, 1H), 9.04 (br, 1H). Anal. Calcd for $C_{44}H_{44}N_2O$: C, 85.67; H, 7.19; N, 4.54. Found: C, 84.20; H, 7.31; N, 4.08.

Results and Discussion

Synthesis and Characterization. The synthetic routes of monomers **M1**−**M8** and polymers **P1**−**P8** are shown in Schemes 1 and 2. All these polymers were easily dissolved in common organic solvents such as chloroform, THF, dichloromethane, and toluene to form good transparent films on glass substrates. The average molecular weights were measured by gel permeation chromatography (GPC) with polystyrene as a standard and THF as an eluting solvent. The related data obtained from GPC are given in Table 1. The number-average molecular weights (M_n) of polymers are between 4900 and 25 200 g/mol, and the polydispersity indexes (PDI) are found between 1.2 and 2.8. The thermal stability of the polymers in nitrogen was evaluated by thermogravimetric analysis (TGA), and their corresponding data are also summarized in Table 1. The TGA analysis indicates that the degradation temperatures (T_d) of 5% weight loss in nitrogen are between 398 and 446 °C. The results of TGA reveal that the polymers are quite stable in nitrogen, and compared with the other polymers (**P2**−**P8**) containing asymmetrical OXD pendants, **P1** containing symmetrical OXD pendants has the lowest T_d. The glass transition temperatures (T_g) and melting temperatures of these polymers were determined by differential scanning calorimetry (DSC) in a nitrogen atmosphere at a scanning rate of 10 °C/min. Their glass transition temperatures are shown between 85 and 148 °C, whereas their melting temperatures are not observed even up to 280 °C. The long flexible alkoxy-substituted OXD polymer, **P5**, has the lowest T_g, and the polar cyano-substituted OXD polymer, **P6**, demonstrates the highest T_g. In contrast to **P1** containing symmetrical OXD pendants, analogous **P5** containing asymmetrical OXD pendants possesses a lower T_g (34 °C lower). Comparing **P8** with **P2**, when the phenyl group is replaced with bulky a naphthyl group in the terminal group of OXD pendants, an increase of 23 °C in T_g is observed in **P8**. In comparison with the analogous structure without oxadiazole pendants, i.e., poly(fluorene phenlyene) (PFP),[17] the degradation temperatures of these novel polymers are higher than that of PFP (T_d is 398 °C), and the glass transition temperatures of these polymers are also higher than that of $PFPOC_6$ (T_g is 72 °C).

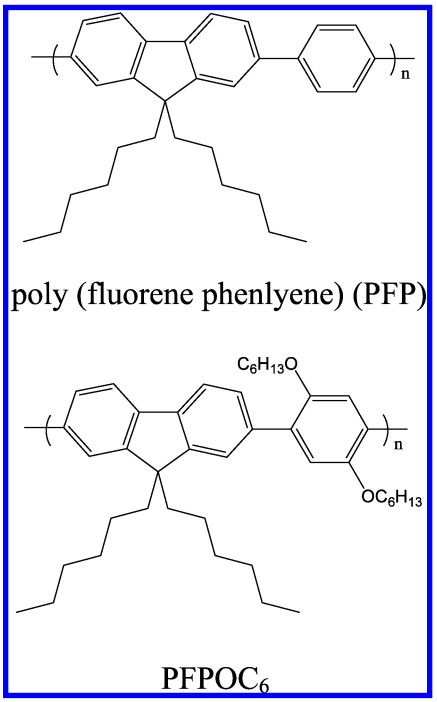

Optical Properties. The photophysical characteristics of the monomers and polymers were studied by PL and UV−vis absorption in both dilute chloroform solutions and thin films. The optical properties of the monomers and polymers are summarized in Tables 2 and 3 and Figures 1−5 serially. It is noted that similar absorption patterns between 250 and 400 nm are observed in various substituted monomers, except **M1**.

Table 2. Absorption and PL Emission Spectral Data of Monomers in Chloroform

monomer	λ_{abs}[a] (nm)	$\lambda_{PL,sol}$[b] (nm)	monomer	λ_{abs}[a] (nm)	$\lambda_{PL,sol}$[b] (nm)
M1	337	418	**M5**	299	372
M2	283	347	**M6**	290	361
M3	286	352	**M7**	302	367
M4	297	370	**M8**	320	379

[a] Wavelength of the maximum absorbance. [b] Wavelength of the maximum PL emission.

Table 3. Absorption and PL Emission Spectral Data of Polymers in Chloroform and in Thin Solid Films

polymer	$\lambda_{abs,sol}$[a] (nm)	$\lambda_{abs,film}$[a] (nm)	band gap[b] (eV)	$\lambda_{PL,sol}$[a] (nm)	$\lambda_{PL,film}$ (nm)	$\Phi_{PL,sol}$[c]	$fwhm_{sol}$ (nm)
P1	321	322	3.14	445	447	0.15	70
P2	327	327	3.33	405	411	0.30	60
P3	329	326	3.32	402	407	0.39	58
P4	325	323	3.32	405	412	0.36	58
P5	322	321	3.33	404	409	0.31	58
P6	323	322	3.32	430	430	0.17	68
P7	323	324	3.33	409	415	0.26	61
P8	328	328	3.34	410	410	0.38	62

[a] Wavelength of the maximum absorbance or PL emission. [b] Band gaps were calculated from the onsets of UV−vis absorption spectra of polymer solutions. [c] PL quantum yield in $CHCl_3$.

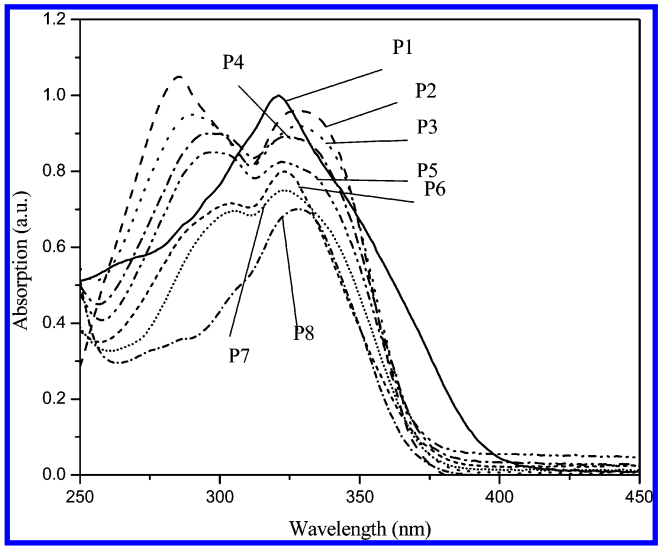

Figure 1. UV−vis spectra of polymer solutions in dilute chloroform.

As expected, both of the absorption and PL spectra are affected by the substituted terminal groups. Compared with those of **M2**, the maximum absorption and PL wavelengths of **M3**−**M8** increase as the polar substituents and π-excessive thiophene (naphthalene) substituents are attached to the OXD rings. Interestingly, compared with that of **M4** ($\lambda_{PL,sol}$ = 370 nm) containing a OMe pendant terminal group, the emission wavelength of **M6** ($\lambda_{PL,sol}$ = 361 nm), in which the polar cyano group is attached to the OXD segment, is not efficiently enlarged. This phenomenon is contrary to our previous study, where the cyano group attached to the chromophoric core will elongate the conjugation and result in a longer emission wavelength.[18] Whereas, the PL emission spectra of the polymers have shown that the cyano-substituted polymer **P6** has a longer emission wavelength ($\lambda_{PL,sol}$ = 430 nm) than that of the alkoxy-substituted polymer **P4** ($\lambda_{PL,sol}$ = 405 nm).

The absorption spectra of synthesized polymers in dilute solutions (chloroform) are depicted in Figure 1.

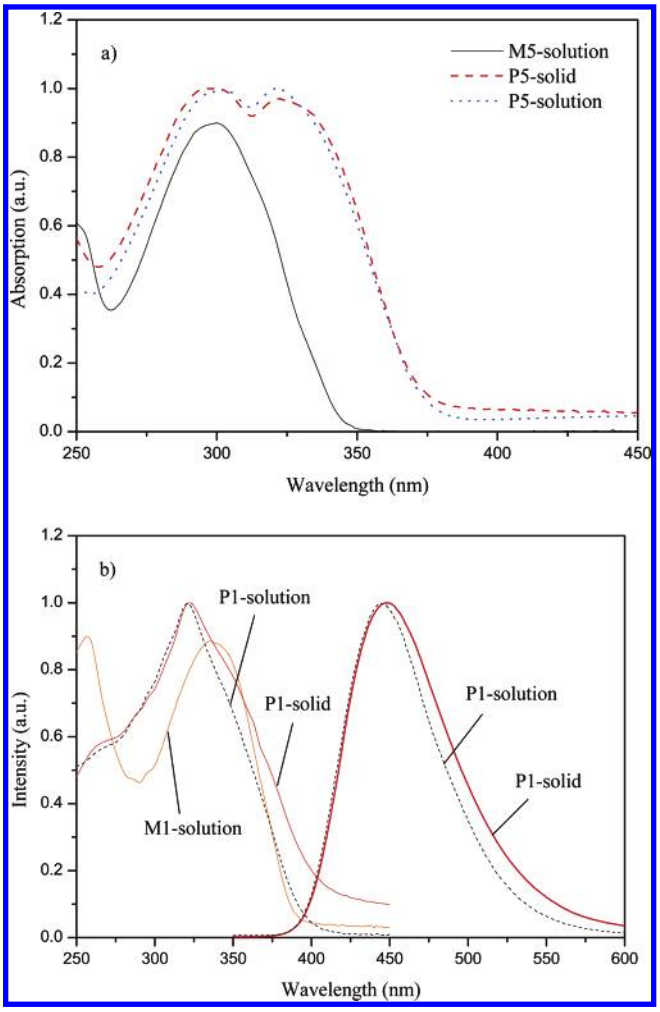

Figure 2. (a) UV−vis spectra of **M5** and **P5**. (b) UV−vis and PL emission spectra of **M1** and **P1**.

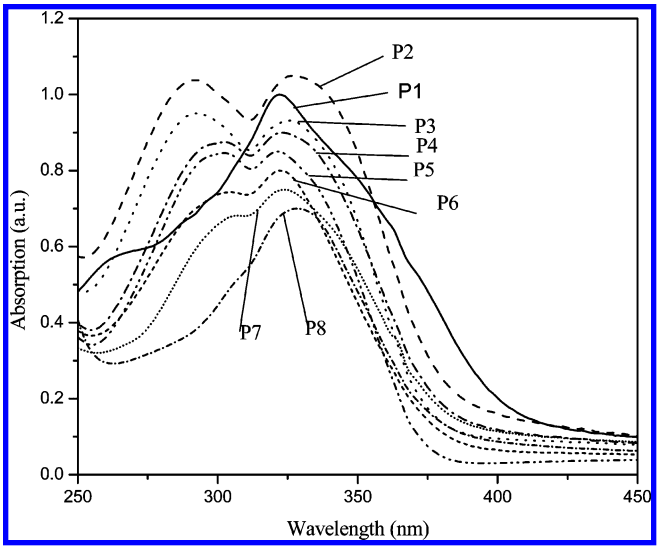

Figure 3. UV−vis spectra of polymer films.

It is noticed that the polymers with asymmetric OXD pendants exhibit two absorption peaks, except **P8**. The absorption spectrum of **P8** shows only one peak, which may be due to the overlap of absorption peaks in both OXD pendants and polymer main chains. The shorter absorption ranging at 290−305 nm is originated from the absorption of the conjugated OXD segments, which is confirmed by the same maximum absorption of

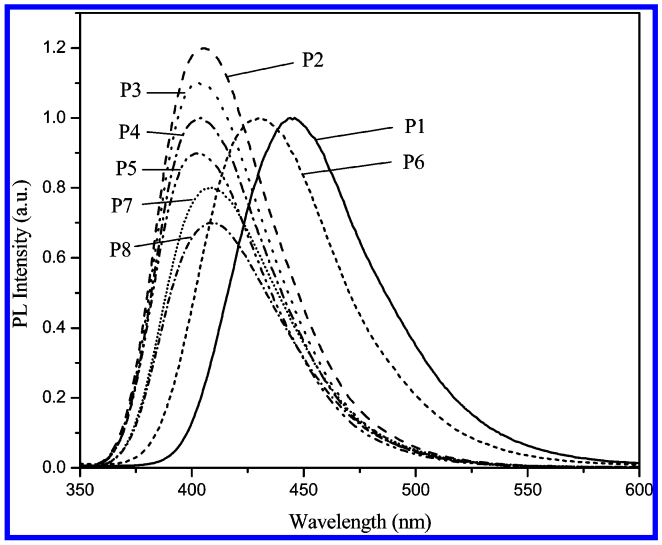

Figure 4. PL spectra of polymer solutions in dilute chloroform.

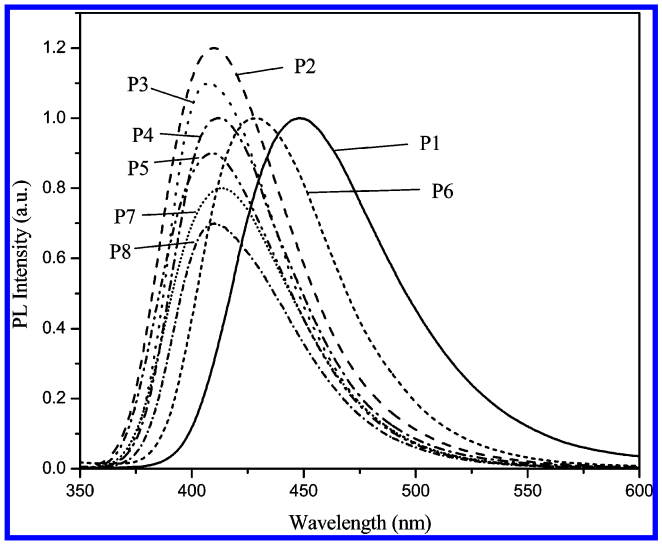

Figure 5. PL spectra of polymer films.

polymer **P5** and monomer **M5** (Figure 2a). The identical absorption maximum of the OXD segment in dilute solutions before and after the polymerization suggests that the electronic interactions between the conjugated oxadiazole segments and the polymer backbones are quite limited.[19] The result also implies that part of the conjugated OXD units (the phenyl−oxadiazole−phenyl conjugated unit) in the asymmetrical side-chain structures twist away from the plane of the conjugated polymer backbone. The longer wavelength peak in the region of 310−370 nm is attributed to the electron transition of $\pi-\pi^*$ along the conjugated backbone of the polymer. Comparing Figures 1−3, the polymer main-chain absorption peaks of the solution and film samples (Figure 2a) are almost identical. This result indicates that the conformation of the polymer chains is very similar in both solution and solid states; in addition, the polymer assembly is in a rather disordered state and refrains from aggregation by this molecular design even in the solid state.

The maximum absorption value of **P1** (321 nm) comes from the fluorene backbone, which can be proved by similar maximum absorption values of all polymers **P1**−**P8** (321−329 nm), regardless of various oxadiazole pendant groups in **P1**−**P8**. The absorption strength of OXD segments in **P1** (containing symmetrical OXD pendants) does not appear as a peak but only shows a shoulder around 337 nm (see Figure 2b), which corresponds to the absorption peak of **M1**. This phenomenon illustrates that the fluorene and both symmetrical OXD segments of **P1** do not twist away from the conjugated plane of the polymer backbone and induce an elongated conjugation. In addition, the absorption strength of **P1** does not show any absorption peak in the region of 270−320 nm (which corresponds to **M5** absorption). It implies the conjugated OXD units of **P1** keep better coplanarity and do not twist away from the conjugated plane. We also observe the solid-state absorption spectrum of **P1** (as shown in Figure 2b) has a tail in the low-energy region around 370−600 nm; it also proves that **P1** has a better coplanarity between the symmetrical OXD pendants and the polymer backbone.

Compared with analogous PFP (λ_{abs} = 370 nm), our polymers exhibit blue-shifted absorption maxima (41−49 nm). The blue shifts of the absorption maxima may be ascribed to two reasons. One is that the coplanarity of the polymer backbone is lost due to the asymmetrical bulky substituents, which cause the steric hindrance and induce the distortion of the backbone. Therefore, the conjugation of polymer backbone is interrupted and induces a blue shift of the absorption maximum. The other is that as mentioned previously the OXD pendants act as electron-withdrawing substituents on the side of the polymer backbone. The electron-withdrawing substituted groups decrease the electron density of the polymer backbone and reduce the absorption maximum.[17]

The optical band gap energies obtained from UV−vis absorption in solutions are also given in Table 3. The band gap energies of polymers were determined by the intersection of tangents through the turning point of the lower energy side of the spectrum and the lengthened baseline for each polymer. The optical band gaps of asymmetrical OXD-substituted polymers from the edge absorption of solution samples are almost identical (3.32−3.34 eV), regardless of terminal functional groups (**P2**−**P8**) of OXD pendants. Nevertheless, the symmetrical OXD-substituted polymer (**P1**) has a red-shifted absorption curve and a smaller band gap (3.14 eV). The smaller band gap may be due to the introduction of two electron-withdrawing OXD moieties and/or a better coplanarity between the polymer backbone and the symmetrical substituents in **P1**. In comparison with PFP, all band gap energies of these polymers are larger than that of PFP (2.92 eV).

The fluorescence quantum yield (Φ_{PL}), the PL emission maxima (λ_{PL}), and the full width at half-maximum (fwhm) values are also presented in Table 3. All emission data given here were obtained by the excitation at the maximum absorption peaks. In dilute solutions, all these polymers only show one emission peak ranging from 402 to 445 nm (Figure 4). Emissions from the OXD pendants are not observed, even when polymers are excited at the absorption peak of the OXD pendants. This indicates the existence of efficient energy transfer from the OXD pendants to the polymer backbone. Except **P6**, all asymmetrical OXD-substituted polymer solutions and films have PL emission in the purple region (Figures 4 and 5). Among these purple-emitting polymers, the electron-donating substituted groups (CH_3, OCH_3, and OC_8H_{17}) in **P3**−**P5** do not seem to affect the emission spectra significantly as compared

with that of **P2**. However, in contrast to **P3**−**P5**, when the electron-withdrawing cyano group is introduced into the terminal group of OXD pendants in **P6**, an obvious red shift (about 25 nm) can be observed in the PL spectrum. The symmetrical OXD-substituted polymer (**P1**), apparently, has a longer PL emission wavelength than the other asymmetrical OXD-substituted polymers (**P2**−**P8**). This result may be due to the improvement of the coplanarity between the polymer backbone and the symmetrical OXD pendants and/or the introduction of two electron-withdrawing OXD pendants.

The PL spectra of polymer thin films are shown in Figure 5. These asymmetrical and symmetrical OXD-substituted polymers emit purple and blue color light, respectively. Compared with the spectra of asymmetrical OXD-substituted polymers (**P2**−**P8**) in solutions, the PL emission peaks of solid films only show a small red shift (the maximum red-shifted value is 7 nm). In contrast to the asymmetrical OXD-substituted polymers, the thin film PL peak of **P1** is just red-shifted for 2 nm, but the emission spectrum shows slight tails in the low-energy ends, which may be due to the aggregation of polymer chains in the solid state. The PL quantum yield will be decreaed when pendant groups (side chains) are conjugated with the polymer main chains.[12c,19,20] It may be due to the multifarious conjugated forms which cannot confine the excitons efficiently; hence, the PL quantum yield decreases in the OXD-substituted polymer. It is interesting to note that the PL quantum yield of the symmetrical OXD-substituted polymer (**P1**) is lower than those of asymmetrical OXD-substituted polymers (**P2**−**P8**), which may be due to the different degree of conjugation between the OXD pendants and the backbone in the symmetrical and asymmetrical structures, respectively.

Compared with PFP, side-chain conjugated PPV (OPO−PPV), and cross-conjugated PPE (PPE-PPV),[14c,20b] these OXD-substituted polymers (**P1**−**P8**) exhibit almost identical spectra in the solution and thin film samples. This result is distinct from PFP, OPO−PPV, and PPE-PPV, which have significant red-shifted spectra in the thin film samples as compared with the solution samples. The results demonstrate that the configuration of the OXD-substituted polymers in our study is not affected by the variation of the state in these polymers. It can be understood by the enhanced steric effect between the OXD pendant groups and the polymer backbone, which consequently increases interchain distances and suppresses the formation of aggregation efficiently. In comparison with PFP, the PL spectra of all our polymers (no matter in solution or solid states) exhibit structureless emission spectra; it is different from PFP, which possesses a well-resolved vibronic band in the emission spectrum. This phenomenon suggests that the OXD pendants can efficiently enhance the amorphism of the polymers and reduce the vibronic structures in the solid state.

Klemm and co-workers reported that the full width at half-maximum (fwhm) values of alkoxy-substituted PPV−PPE hybrid polymers strongly depend on the length of the attached side chains.[21] The fwhm value increases from 36 nm in PPV−PPE hybrid polymers containing longer side chains ($-OC_{18}$) to 67 nm in PPV−PPE hybrid polymers containing shorter side chains ($-OC_8$). They explain that the smaller fwhm value of the long side-chain polymers is due to the emission coming from isolated main-chain fluorophores; however, the larger fwhm value of the short side-chain polymers is a contribution of isolated main-chain fluorophores and a certain degree of aggregation. In our synthetic polymers, the fwhm values of the emission curves of the polymers in the solution and solid states are almost independent of the terminal groups (**P2**−**P5** and **P7**−**P8**) of the OXD pendants. Only about 10 nm of increase in the fwhm value was observed in symmetrical **P1** and asymmetrical **P6** (with a strong electron-withdrawing cyano substituent attached to the end of the OXD pendant). The strong polar groups of the cyano terminals in the pendants of **P6** may induce more or less intramolecular and/or intermolecular interactions and consequently broaden the fwhm value. Otherwise, comparing **P5** with **P2**−**P4** of our polymers containing OXD pendants, the fwhm value of the long terminal side-chain polymer (**P5**) is almost identical with those of short terminal side-chain polymers (**P2**−**P4**). From this result, we can generally conclude that the asymmetrical OXD pendants can provide good steric hindrance and reduce aggregation, except OXD pendants containing strong polar cyano groups (such as **P6**). In general, the lowest quantum yields of **P1** (due to the symmetrical pendant structure) and **P6** (due to the strong polar cyano substituent) are also correlated to their largest fwhm values.

In summary of the absorption and PL results, we can conclude the photophysical properties are strongly affected by the OXD pendants. In asymmetrical substituted polymers, the absorption maximum peaks and optical band gaps are almost independent of the electronic effect (electron-withdrawing group, −CN, electron-donating group, −R or −OR) and size effect (the size of the terminal functional group) of the substituted OXD pendants. However, the PL emission peaks and the quantum yields are affected by the electronic effect. When the strong electron-withdrawing cyano group is attached to the terminal phenyl group of the OXD pendant, the PL emission peak is red-shifted and the quantum yield is reduced. Except **P6**, these polymers have similar PL emission peaks as that of PFP ($\lambda_{abs,sol}$ = 408 nm, $\lambda_{abs,film}$ = 422 nm), but they show larger Stokes shifts than that of PFP. As a symmetrical OXD-substituted polymer, **P1** has an almost identical absorption maximum value as those of asymmetrical substituted polymers, but relatively it possesses a longer PL emission peak and a lower quantum yield.

Electrochemical Properties. To fit the energy band structural scheme of PLED device, it is necessary to determine the energy levels of the highest occupied molecular orbital (HOMO) and the lowest unoccupied molecular orbital (LUMO) of each component, which was carried out by CV to investigate the redox behavior of the polymer thin films. The potential estimated here was based on the reference energy level of ferrocene (4.8 eV below the vacuum level) according to the following equation:[21] $E^{HOMO}/E^{LUMO} = [-(E^{onset} - 0.45) - 4.8]$ eV. The onset potentials were determined from the intersection of two tangents drawn at the rising and background currents of the cyclic voltammogram. A crude estimation of the LUMO levels of reduction polymers were deduced from the HOMO values and the optical band gaps.

These polymers have the same backbone structure of poly(fluorene-*co*-*alt*-phenylene) with different substituents on the OXD pendants which are attached to the phenylene groups. It is interesting to evaluate that how do these OXD pendants modulate the electrochemical

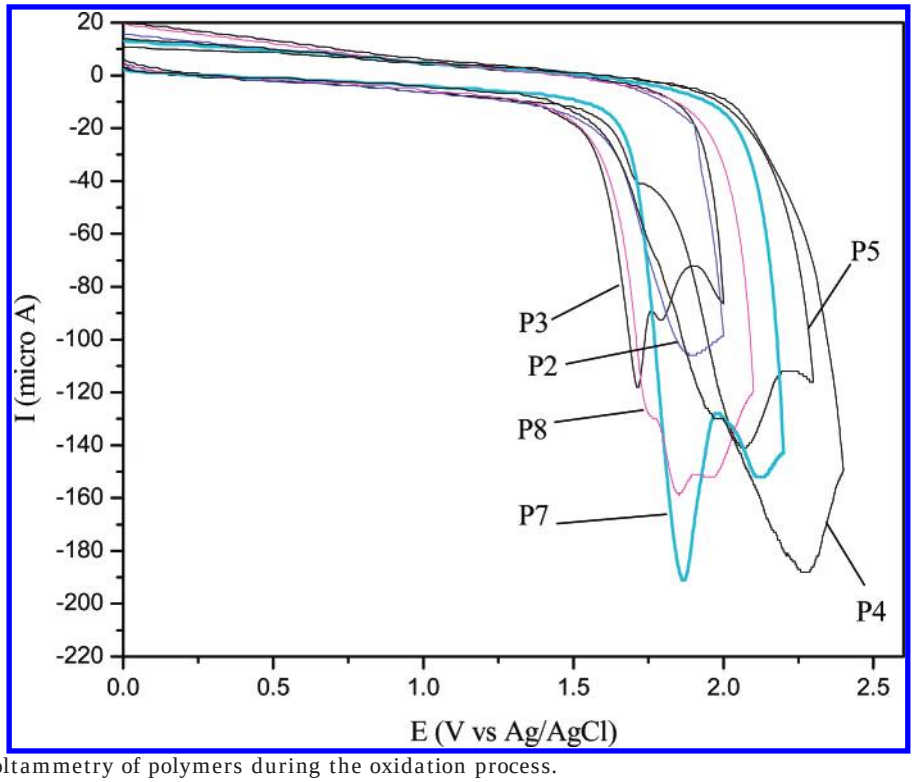

Figure 6. Cyclic voltammetry of polymers during the oxidation process.

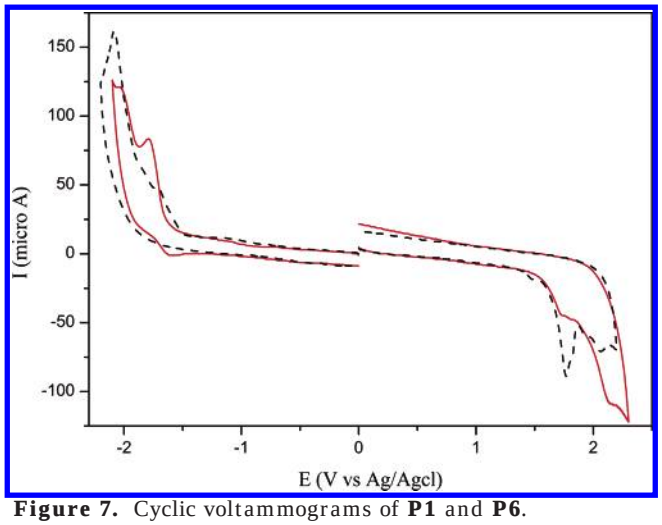

Figure 7. Cyclic voltammograms of **P1** and **P6**.

behavior of these polymers. As shown in Figures 6 and 7, most of the polymers possess two anodic peaks, which can be attributed to two different blocks in the OXD pendants and polymer backbones of the copolymers, respectively. Since the reduction potentials are difficult to be measured, only **P1** and **P6** can be determined, which may be due to their strong electron-withdrawing property. The asymmetrical substituted polymers (**P2**−**P5**) show oxidized peaks irreversibly at potentials ranging from 1.72 to 1.98 V (Table 4) and the onset potentials of oxidation between 1.57 and 1.62 V in the anodic scan. Comparing **P3**−**P5** with **P2**, it seems that the electron-donating groups slightly reduce the overall electron-withdrawing effect of the OXD pendants. Compared with **P2**, the oxidized onset potentials of **P7** and **P8** are not remarkably changed by the replacement of the phenyl group with the π-excessive thiophene and naphthalene groups.

As for **P6** with cyano-substituted OXD pendants, the oxidation onset potential is 1.39 V and reduction onset potential is −1.51 V. It is obvious that **P6** is much easier to be reduced than the other polymers; this is probably due to the strong electron-withdrawing cyano group which increases the overall electron-withdrawing effect of OXD pendants. Compared with **P2**, the HOMO energy level of **P6** can be easily adjusted for 0.4 eV by changing the terminal functional groups of OXD pendants with CN terminals. As for the symmetrical OXD-substituted polymer (i.e., **P1**), the oxidation onset potential is 1.74 V and reduction onset potential is −1.65 V. The band gap obtained from the difference of onset potentials between the reduction and oxidation processes is estimated to be 3.20 V, which is close to that obtained from the absorption edge in the UV−vis spectrum (3.14 V).

Table 4. HOMO and LUMO Energies and Electrochemical Properties of Polymers

polymer	$E^{red/onset}$ (V)	$E^{red/peak}$ (V)	$E^{ox/onset}$ (V)	$E^{ox/peak}$ (V)	E^{HOMO} (eV)	E^{LUMO} (eV)
P1	−1.65	−1.79	1.55	1.74	−5.90	−2.70[a]
P2			1.62	1.90	−5.97	−2.64[b]
P3			1.57	1.72	−5.92	−2.60[b]
P4			1.58	1.98	−5.93	−2.61[b]
P5			1.61	1.73	−5.96	−2.63[b]
P6	−1.51	−1.72	1.39	1.50	−5.74	−2.84[a]
P7			1.69	1.87	−6.04	−2.71[b]
P8			1.60	1.77	−5.95	−2.61[b]

[a] LUMO Energies were obtained from the cyclic voltammetry. [b] LUMO Energies were deduced from HOMO values and optical band gaps.

The OXD pendants act as electron-withdrawing substituents on the backbones of poly(fluorine-*co*-*alt*-phenylene)s and thus decrease the LUMO levels (−2.60 to −2.84) of all polymers as compared to that of PFP (HOMO = −5.36, LUMO = −2.47). The lower LUMO potentials of these polymers indicates that the incorporation of electron-withdrawing OXD pendants increases the electron affinities and reduces the LUMO levels of wide band gap polymers (such as PFP) to match the

Table 5. EL Data of PLED Devices[a]

polymer	$\lambda_{max,EL}$ (nm)	V_{on}[b] (V)	V_{on}[c] (V)	max brightness (cd/m^2)
P1	452	7.5	7.5	126
P2	408	7.5	7.5	29
P3	409	7.5	7.5	51
P4	423	8.5	8.5	104
P5	406	8.5	9.0	376
P6	431	6.5	7.0	306
P7	416	7.0	7.0	82
P8	417	6.5	7.0	462

[a] Device structure: ITO/PEDOT:PSS/polymer/Ca/Al. [b] V_{on} is the turn-on voltage of current. [c] V_{on} is the turn-on voltage of light.

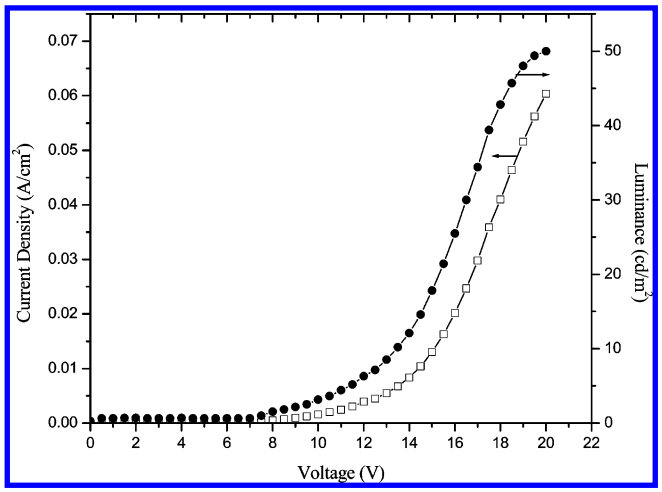

Figure 8. Current−voltage and luminescence−voltage characteristics of ITO/PEDOT:PSS/P3/Ca/Al device.

work function of the cathode. From these results, we can conclude that both HOMO and LUMO energy levels can be adjusted not only by the OXD pendants of the polymer backbone but also by the attached functional groups of the OXD pendants.

Electroluminescent (EL) Properties of PLED Devices. The CV and UV−vis results show that both HOMO and LUMO energy levels of our new polymers do not match the work functions of indium−tin oxide (ITO) anode and Al cathode. Therefore, we choose PEDOT and Ca as the anode and cathode, respectively, to overcome these large energy barriers. A series of double-layer EL devices with the configuration of ITO/PEDOT:PSS/Polymer/Ca/Al were made by spin-coating the polymer solutions (with a concentration of 10 mg/mL) onto PEDOT-coated glass substrates, and their EL data are demonstrated in Table 5.

The current−voltage and luminescence−voltage, i.e., EL response, curves of one typical PLED device (ITO/PEDOT:PSS/P3/Ca/Al) are displayed in Figure 8. All these devices show turn-on voltages for current from 6.5 to 8.5 V and turn-on voltages for light from 7 to 9 V (shown in Table 5). Compared with **P2** without flexible ends on OXD pendants, **P5** with OC_8 terminals on OXD pendants has a higher turn-on voltage. This result may be due to the intrinsic insulation property of the long alkoxy side chains in **P5** which consequently increases the turn-on voltage. The attainable maximum luminance is 462 cd/m^2 at 15 V for **P8** as an emitter. These similar turn-on voltages for current and light illustrate that a matched balance of injection and transportation in charge is achieved. The balanced injection and transportation of both charge carriers may be due to the limited electronic interactions between the cross-

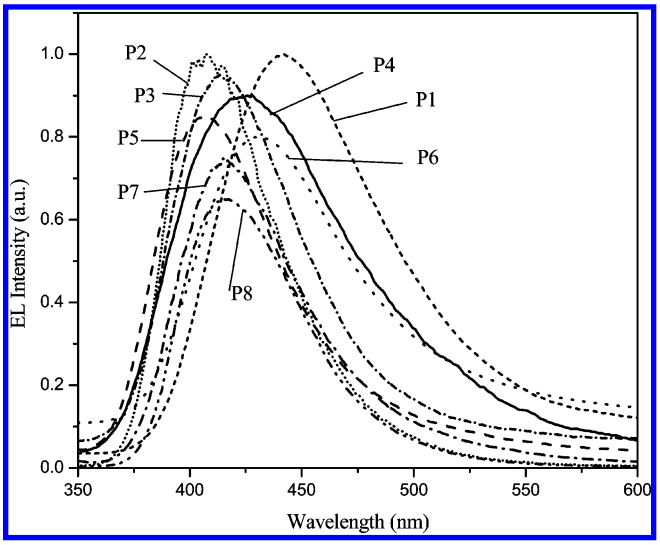

Figure 9. Normalized EL spectra of ITO/PEDOT:PSS/Polymer/Ca/Al devices.

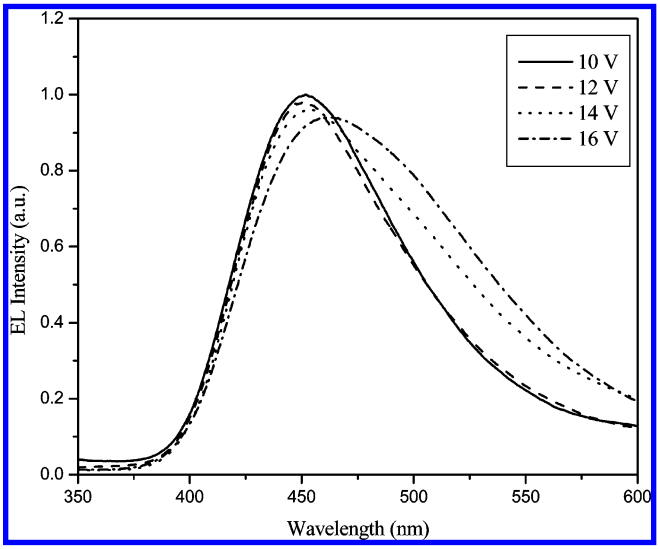

Figure 10. Normalized EL spectra of ITO/PEDOT:PSS/P1/Ca/Al device at different voltages.

conjugated OXD pendants and the conjugated polymer backbone.[15c]

As shown in Figure 9, these devices of asymmetrical OXD-substituted polymers give purple to blue emission colors, and the EL emission peaks are between 406 and 452 nm (Table 5). The EL emission peaks, general speaking, are well matched with the corresponding PL emission peaks of the thin films (Table 4). This indicates that the similar radiative excited states are involved in both EL and PL processes. In contrast to all asymmetrical OXD-substituted polymers, the emission spectra (Figure 10) of **P1** at different voltages are slightly voltage-dependent. Since the absorption and fluorescence data reveal that **P1** forms excimers due to the aggregation in the solid film, the EL spectra of **P1** are red-shifted and become broader by increasing voltage.

Conclusion

A series of soluble alternating fluorene-based copolymers with OXD pendants were synthesized by the palladium-catalyzed Suzuki coupling reaction. These polymers exhibit good thermal stability up to 400 °C and possess higher glass transition temperatures than

that of the analogous dialkoxy-substituted polymer ($PFPOC_6$) consisting of the same backbone without OXD pendants. Their photophysical and electrochemical properties are not only affected by the OXD pendants but also affected by the terminal functional groups. Owing to the large steric hindrance of OXD pendants, the aggreagation of these polymers in solid state is reduced, which results in almost identical PL emissions in both solution and solid states. The incorporation of OXD pendants into polymer backbone leads to mitigating the interchain interaction and improving the electron affinity and charge-injection properties effectively. Since only one emission peak is observed in both PL and EL spectra of these polymers, it is evidenced that effective energy transfer from the OXD pendants to the conjugated polymer backbones has occurred, thus eliminating the light emission from the OXD pendants. By comparing **P1** with **P5**, we recognize that asymmetrical OXD-substituted polymers possess better properties (higher quantum yield and lower aggregation in the solid state) than the symmetrical OXD-substituted polymer. The symmetrical OXD-substituted polymer (**P1**) has a longer PL emission wavelength than the asymmetrical OXD substituted polymers (**P2**−**P8**), which may be due to the improvement of the coplanarity between the polymer backbone and the symmetrical OXD pendants and/or the introduction of two electron-withdrawing OXD pendants.

Acknowledgment. We thank the financial support from the National Science Council of Taiwan (ROC) through NSC 92-2113-M-009-016.

References and Notes

(1) Burroughes, J. H.; Bradley, D. D. C.; Brown, A. R.; Marks, R. N.; Mackay, K.; Friend, R. H.; Burn, P. L.; Holmes, A. B. *Nature (London)* **1990**, *347*, 539.
(2) (a) Kraft, A.; Grimsdale, A. C.; Holmes, A. B. *Angew. Chem., Int. Ed.* **1998**, *37*, 402. (b) Friend, R. H.; Gymer, R. W.; Holmes, A. B.; Burroughes, J. H.; Marks, R. N.; Taliani, C.; Bradley, D. D. C.; dos Santos, D. A.; Bredas, J. L.; Lögdlund, M.; Salaneck, W. R. *Nature (London)* **1999**, *397*, 121. (c) Johnson, M. J.; Sempel, A. *Inf. Disp.* **2000**, *2*, 12.
(3) (a) Gustafsson, G.; Cao, Y.; Treasy, G. M.; Klavetter, F.; Colaneri, N.; Heeger, A. J. *Nature (London)* **1992**, *357*, 477. (b) Greenham, N. C.; Friend, R. H. *Solid State Phys.* **1995**, *49*, 1.
(4) (a) Liu, M. S.; Jiang, X.; Liu, S.; Herguth, P.; Jen, A. K. Y. *Macromolecules* **2002**, *35*, 3532. (b) Jenekhe, S. A.; Osaheni, J A. *Science* **1994**, *265*, 765.
(5) Krebs, F. C.; Jorgensen, M. *Macromolecules* **2002**, *35*, 7200.
(6) Chen, Z. K.; Meng, H.; Lai, Y. H.; Huang, W. *Macromolecules* **1999**, *32*, 4351.
(7) Marsella, M. J.; Fu, D. K.; Swager, T. M. *Adv. Mater.* **1995**, *7*, 145.
(8) Gillissen, S.; Jonforsen, M.; Kesters, E.; Johansson, T.; Theander, M.; Andersson, M. R.; Inganas, O.; Lutsen, L.; Vanderzande, D. *Macromolecules* **2001**, *34*, 7294.
(9) (a) Cui, Y.; Zhang, X.; Jenekhe, S. A. *Macromolecules* **1999**, *32*, 3824. (b) Jandke, M.; Strohriegl, P.; Berleb, S.; Werner, E.; Brutting, W. *Macromolecules* **1998**, *31*, 6434.
(10) (a) Jenekhe, S. A.; Zhang, X.; Chen, X. L.; Choong, V. E.; Gao, Y.; Hsieh, B. R. *Chem. Mater.* **1997**, *9*, 409. (b) Jen, A. K.; Wu, X. M.; Ma, H. *Chem. Mater.* **1998**, *10*, 3824.
(11) (a) Zhang, X.; Jenekhe, S. A. *Mater. Res. Soc. Symp. Proc.* **1998**, *488*, 539. (b) Wang, Y. Z.; Gebler, D. D.; Fu, D. K.; Swager, T. M.; MacDiarmid, A. G.; Epstein, A. J. *Synth. Met.* **1997**, *85*, 1179.
(12) (a) Wang, C.; Jung, G. Y.; Hua, Y.; Pearson, C.; Bryce, M. R.; Petty, M. C.; Batsanov, A. S.; Goeta, A. E.; Howard, J. A. K. *Chem. Mater.* **2001**, *13*, 1167. (b) Zhan, X.; Liu, Y.; Wu, X.; Wang, S.; Zhu, D. *Macromolecules* **2002**, *35*, 2529. (c) Lee, Y. Z.; Chen, X.; Chen, S. A.; Wei, P. K.; Fann, W. S. *J. Am. Chem. Soc.* **2001**, *123*, 2296. (c) Peng, Z.; Zhang, J. *Chem. Mater.* **1999**, *11*, 1138. (d) Chung, S. J.; Kwon, K. Y.; Lee, S. W.; Jin, J. L.; Lee, C. H.; Lee. C. E.; Park, Y. *Adv. Mater.* **1998**, *10*, 1112. (e) Kim, J. H.; Park, J. H.; Lee. H. *Chem. Mater.* **2003**, *15*, 3414.
(13) Adachi, C.; Tsutsui, T.; Saito, S.*Appl. Phys. Lett.* **1990**, *56*, 799.
(14) (a) Ruiz, J. P.; Dharia, J. R.; Reynolds, J. R.; Buckley, L. J. *Macromolecules* **1992**, *25*, 849. (b) Chen, Z. K.; Meng, H. Lai, Y. H.; Huang, W. *Macromolecules* **1999**, *32*, 4351. (c) Meng, H.; Yu, W. L.; Hunang, W. *Macromolecules* **1999**, *32*, 8841. (d) Pu, Y. J.; Soma, M.; Kido, J.; Nishide, H. *Chem. Mater.* **2001**, *13*, 3817. (e) Chen, Z. K.; Lee, N. H. S.; Huang, W.; Wu, Y. S.; Cao, Y. *Macromolecules* **2003**, *36*, 1009. (f) Wu, F. I.; Reddy, S.; Shu, C. F.; Liu, M. S.; Jen, A. K. Y. *Chem. Mater.* **2003**, *15*, 269.
(15) (a) Moratti, S. C.; Cervimi, R.; Holmes, A. B.; baigent, D. R.; Friedn, R. H.; Greenham, N. C.; Gruner, J.; Hamer, P. J. *Synth. Met.* **1995**, *71*, 2117. (b) Yang, J. S.; Swager, T. M. *J. Am. Chem. Soc.* **1998**, *120*, 5321.
(16) Bo, Z.; Zhang, C.; Severin, N.; Jurgen, P. R.; Schluter, A. D. *Macromolecules* **2000**, *33*, 2688.
(17) Liu, B.; Yu, W. L.; Lai, Y. H.; Huang, W. *Chem. Mater.* **2001**, *13*, 1984.
(18) Song, H. H.; Lin, H. C. *Liq. Cryst.* **2004**, *31*, 831.
(19) Xu, B.; Pan, Y.; Zhang, J.; Peng, Z. *Synth. Met.* **2000**, *114*, 337.
(20) Liu, M. S.; Jiang, X.; herguth, P.; Jen, A. K. Y. *Chem. Mater.* **2001**, *13*, 3820. (b) Wilson, J. N.; Windscheif, P. M.; Evans, U.; Myrick, M. L.; Bunz, U. H. F. *Macromolecules* **2002**, *35*, 8681.
(21) Egbe, D. A. M.; Cornelia, B.; Nowotny, J.; Gunther, W.; Klemm, E. *Macromolecules* **2003**, *36*, 5459.

MA0489927